Computational Analyses of Waveguide PIN Phase-Shifters in SOI

A Project Report

submitted by

VIVEK P S

in partial fulfilment of the requirements
for the award of the degree of

MASTER OF TECHNOLOGY

DEPARTMENT OF ELECTRICAL ENGINEERING
INDIAN INSTITUTE OF TECHNOLOGY MADRAS.

MAY 2014

THESIS CERTIFICATE

This is to certify that the thesis titled **Computational Analyses of Waveguide PIN Phase-Shifters in SOI**, submitted by **Vivek P S**, to the Indian Institute of Technology, Madras, for the award of the degree of **Mater of Technology**, is a bonafide record of the research work done by him under my supervision. The contents of this thesis, in full or in parts, have not been submitted to any other Institute or University for the award of any degree or diploma.

Dr. Bijoy K. Das
Project Guide
Associate Professor
Dept. of Electrical Engineering
IIT-Madras, India, 600 036

Place: Chennai, India
Date: 5th may 2014

Dedicated to my Parents

ACKNOWLEDGEMENTS

I would like to thank all those who supported me during my project work providing knowledge and suggestions. First of all, I would like to thank my project guide Dr. Bijoy Krishna Das, who accepted me for doing project under him. In addition to that the personal discussions with him really helped me in the progress and successful completion of my project. My project work was carried out in Integrated Optoelectronics laboratory IIT-Madras, the group have done remarkable research in the area of Silicon photonics. I am grateful to each and every member in the group. I would like to thank M.Chaitanya kumar who gave me the basic idea of numerical computation techniques and handed over the batton of his work to continue the same, D. Dadavali and Sakthivel P for helping me in doing Medici simulations and discussion of experimental results. Sujith Chandran who is one of the PhD students in our lab, his pin point arguments helped me correcting the mistakes during the course of project and I am thankful for his mentoring and care. Saket Kaushal who is one of the MS students in our lab helped patiently for doing simulations in Lumerical mode solver and supported me in all sort of occasions for the successful completion of my project. Mandar Belambe , dual degree student helped whenever I faced computationally related issues and I would like to acknowledge him in this occasion. Sreevatsa Kurudi, MS student helped me in various occasions in the simulations as well as theoretical discussions.

I express my gratitude to Meenatchi Sundaram, Sidharth R, Harish Sasikumar, Rashmi Joshi, Riddhi Nandi, Sumi R, Sireesha Nambigari, Deepak kumar, Seetha lakshmi who are part of Integrated Optoelectronics team and they gave good motivation for me in the group discussions and helped in providing facilities for doing simulations. I would like to thank Shantanu Pal and Parimal Sah , who are PhD scholars and they gave positive suggestions during the progress of my project.

I got enormous support from outside the Integrated optoelectronic group. I am grateful to Prasanth Kumar M, who helped me by providing resources and familiarizing Matlab tool for simulations. I would thank Nikhil K S, Anwar A and Sarath G for helping me in various occasions of my project. Finally I should admit that, I got enormous support from my family for the successful completion of M.Tech.

ABSTRACT

The computation and performance analyses of PIN waveguide phase-shifters in SOI platform have been carried out. Poisson's and Maxwell's equation solvers have been used to solve the electrical and optical characteristics respectively. Presently there are no reliable and efficient simulators available which can solve both electrical and optical characteristics simultaneosly. The steady state as well as transient electrical and optical behavior of PIN phase-shifter for injection mode operation on various waveguide dimensions were carried out. In addition to that steady state self heating (Joule heating) effect on phase shifting application have been analyzed using Fourier heat conduction equation.

The computed results show figure of merit $V_\pi L_\pi = 0.204$ V-mm and carrier rise (fall) time $\tau = 60.3ns(45.3ns)$, for a waveguide width W $\sim 5\mu m$. For reduced waveguide width of $\sim 2\mu m$, the figure of merit and carrier rise (fall) time have been evaluated as 0.189 V-mm and 4.8 ns(0.12ns) respectively. These results have been compared with the simulation results obtained using various commercial simulators like T-CAD Medici and Lumerical mode solver.

Further, the steady state self-heating studies of the device shows that at higher forward bias point (1.2V), thermo-optic effect dominates over plasma dispersion effect. The self heating results of the simulator have been compared with practical results of PIN phase-shifter fabricated in our labs.

TABLE OF CONTENTS

LIST OF FIGURES

ABBREVIATIONS

Acronyms

CMOS	Complimentary metal-oxide semiconductor
MOS	Metal-oxide semiconductor
SRH	Shockley Read Hall
TE	Transverse Electric (polarization)
TM	Transverse Magnetic (polarization)
Si	Silicon
SiO_2	Silicon dioxide

Units

MHz	Mega Hertz
GHz	Giga Hertz
$\boldsymbol{\mu m}$	Micrometer
ns	Nano Second
A	Ampere
V	Volt
μm	Micro meter
mm	milli meter

NOTATION

$\mathbf{n}$	Refractive index
$\mathbf{n}_{eff}$	Effective refractive index
$\boldsymbol{\epsilon}$	Permittivity
L_{pi}	Length for achieving π phase
$\boldsymbol{\alpha}$	Absorption coefficient
n, p	Electron and Hole concentrations
(i, j)	represents the node at (i,j) incremental distance from origin
n,p	Electron and Hole concentrations
V	Potential
δ	correction factor

CHAPTER 1

Introduction

The impact of "electronics" made considerable change in the day to day life of mankind. The applications of electronics became an integral part of different areas of science and technologies like computing , biomedical, instrumentation, sensing and telecommunications. We know that the evolution of electronics started after the invention of integrated chip (IC), which helped to make compact and high speed devices for various applications. Considering the past two decades transistor count per chip is increasing from ten millions to thousands of million [1] .

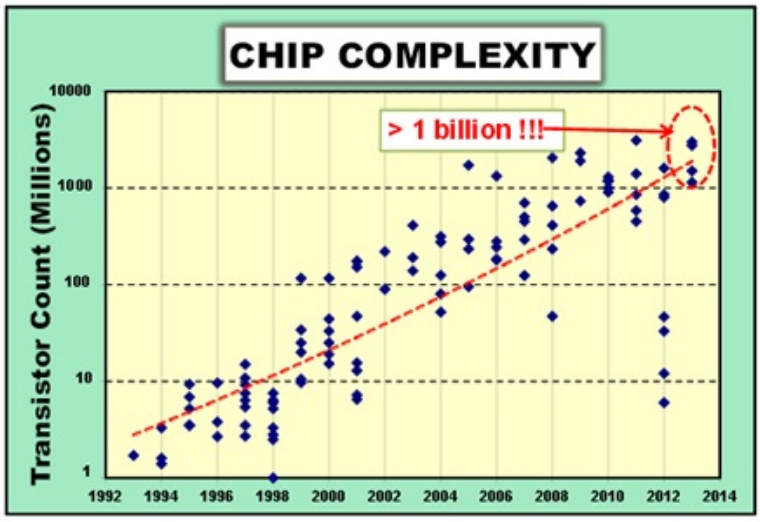

Figure 1.1: Number of transistors per chip is increasing over the years [1].

These transitors are interconnected using copper or aluminium. As the number of transistors in a chip increases resulting the reduction in spacing between them which effectively reduces the cross sectional area of interconnects. As the interconnect is scaling down the resistance of the interconnect increases. The pitch (spacing between two metal interconnect) also reduces while scaling down, this will increase the capacitance of the system. The RC-time constant will increase considerably, thus the over all delay increases which will limit the bandwidth of operation of the device [2]. In addition

to that the power density of a chip is also increasing considerably[3]. Thus heating is another major problem in electronics integrated circuit.

So far we are discussing the major bottlenecks that seriously affecting the electronics related systems. One good solution for these issues is to replace the electrical interconnect by optical interconnect. Here the possibilities of silicon photonics can be effectively applied.

1.1 Silicon photonics

Silicon photonics mainly deals with study and application of on chip photonic devices in which silicon is used as medium for light. As in electronics system, photonic devices are also divided as active and passive. The following figure 1.2 shows system for on chip optical interconnect between cores or logic cells. The electrical signal (data) can

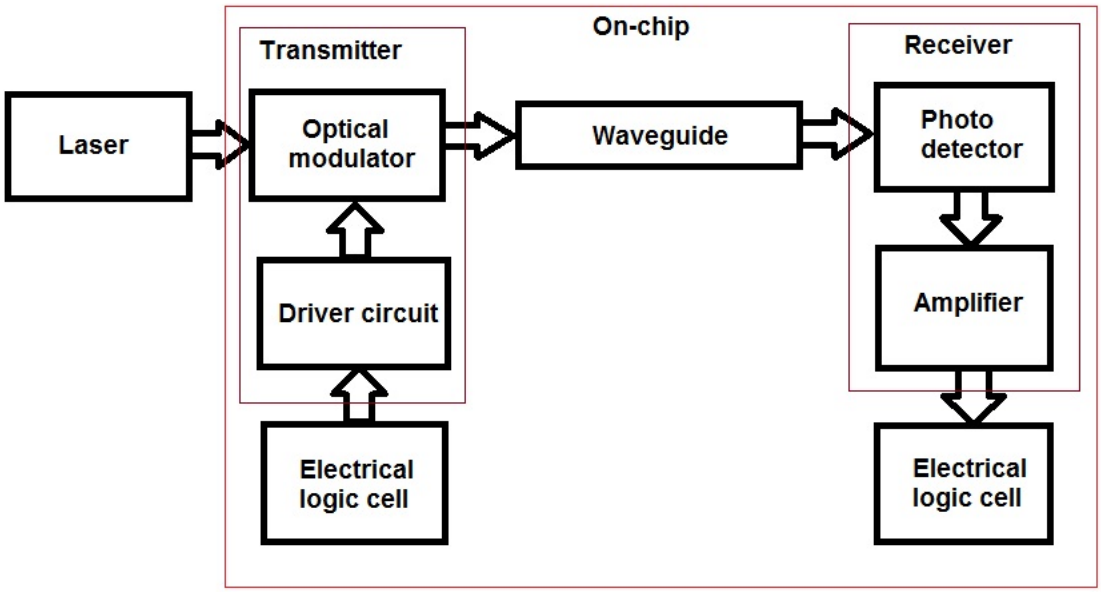

Figure 1.2: Schematic for on chip optical interconnect between cores or logic cells.

be encoded into laser light (optical signal) with the help of a driver circuit and a modulator. The modulated signal then guided through a waveguide and then detected and converted back to the electrical signal(data). Here, both active optoelectronic elements modulator,detector and passive element waveguide can be made of silicon. These are

the basic building blocks of an electro-optic system. Silicon on insulator (SOI) is an excellent material platform for the electronic as well as photonic industry. SOI has low parasitic effects and absence of latch up [4,5,6], these are good properties as far as electronic devices are concerned. As far as photonic devices are concerned, SOI is a good material for the guided wave optics, because silicon has a better refractive index contrast with SiO_2 and air. This will give better confinement for the modes inside the waveguide. Moreover the silicon is transparent to the wavelength above $1.1\mu m$, thus waveguide based devices on SOI can be used for communication applications over the bandwidth C,L and S. Besides optical waveguides based on SOI can be fabricated using CMOS processing technology for high speed systems [7].

As far as optoelectronic devices are concerned modulators are the key element in electro-optic conversion. The following part discussing the different modulation mechanisms and different modulator configurations.

1.2 Basic Modulation Mechanisms

Electro - optic modulation is a process by which super imposing the electrical data over optical carrier signal using digital line coding technique.

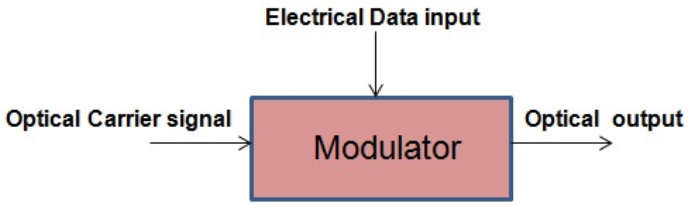

Figure 1.3: General Block diagram for an electro-optic modulator.

There are two main types of waveguide based modulator configurations used,

i.Mach-Zehnder configuration

ii.Ring resonator configuration

Mach-Zehnder configuration: The operation mechanism is as follows when a light beam is coupled to the input port of the MZI, it equally splits in to two and guided

through respective arms. The light which is guided through the phase shifter is modulated according to the external input. The light which is being guided by the other arm acquires a phase shift only due to the path which has traveled. These two guided waves interfere at the combiner of MZI constructively or destructively according to their phase relationships.

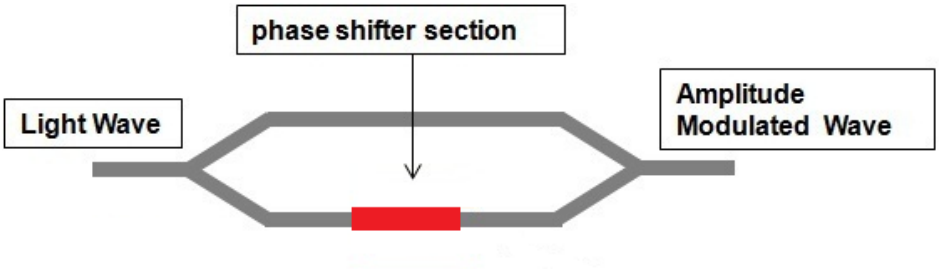

Figure 1.4: Mach-Zehnder configuration for modulator [18].

Ring resonator configuration: The schematic view of a ring resonator modulator is shown in figure 1.5. There are two waveguides in which one is straight and the other one is ring shaped. The light launched in straight waveguide will couple maximum to the ring whenever the phase is matching (resonant to the wavelength) to it during the propagation. At critical coupling the throughput will be minimum. This type of configuration can be used for making delay lines in optical circuit.

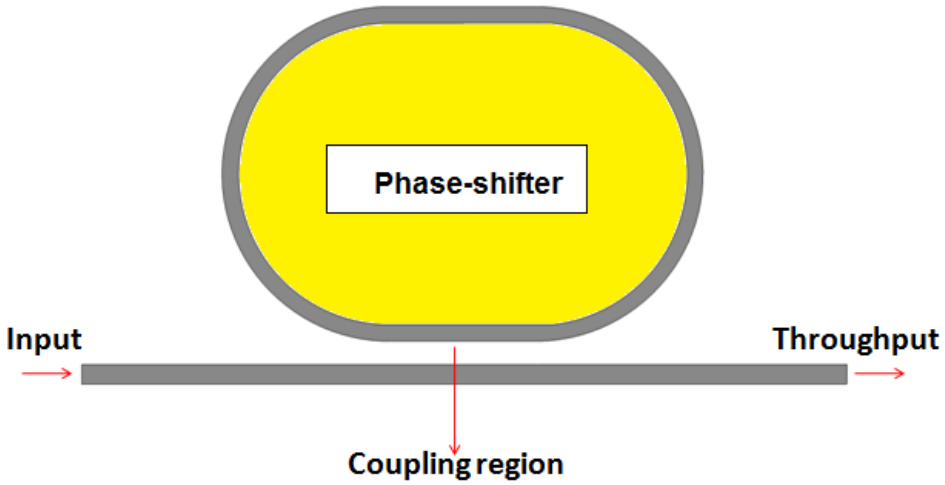

Figure 1.5: Ring resonator configuration for modulator.

The resonant wavelength of the system can be tuned if we change the phase of the signal inside the ring.

The electro optic modulation can be effectively achieved through the "phase shifting" of the carrier, which has been discussed in the second chapter. The phase modulation of light in a waveguide is accomplished by changing the refractive index of the waveguide medium through the physical effects such as Kerr effect[8], Frandz-Keldysh effect[9], Thermo optic effect[10], plasma disperrsion effect[11]. In crystalline silicon, the plasma dispersion and thermo-optic effects are strong and the other physical effects are negligible, which is due to the centro symmetric nature in the crystal lattice of silicon.

1.3 Plasma dispersion effect

The "Plasma dispersion effect" is most common technique used to achieve the phase modulation in silicon. This effect can be achieved by varying the free carrier concentration through various mechanisms such as carrier accumulation, injection or depletion.

Carrier Accumulation: The schematic view of accumulation type modulator is shown in figure 1.6, which utilizes the accumulation of the majority carriers. In the

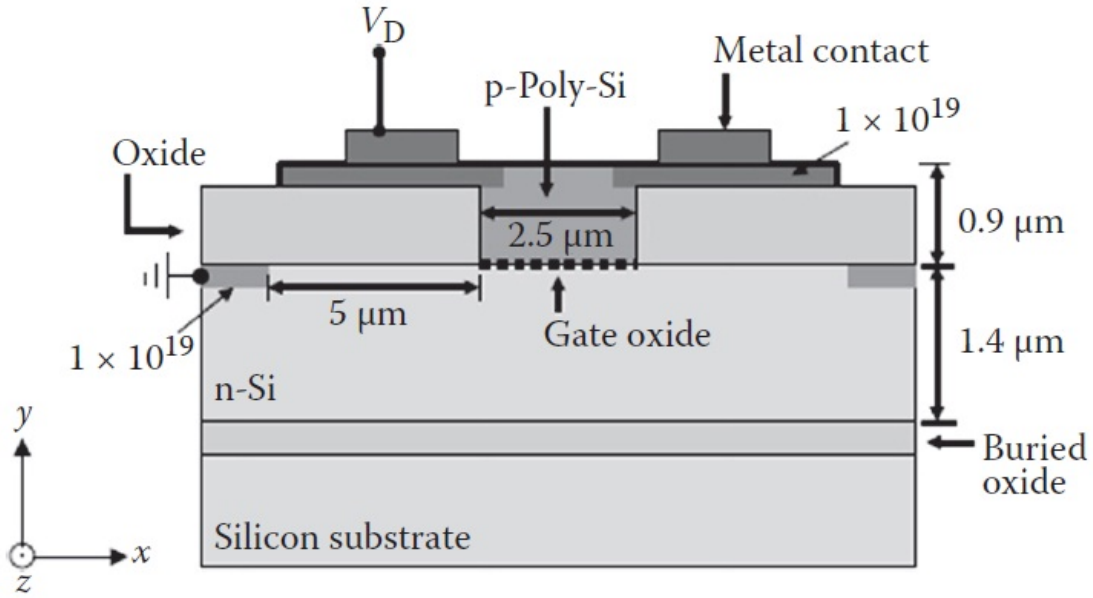

Figure 1.6: Cross-sectional view of MOScap-ribwaveguide based modulator in SOI platform [12].

figure 1.6, the substrate or body is lightly doped with n type dopant with a thin gate oxide and p-type polysilicon gate forming a MOS capacitor rib waveguide structure. The two outer edges of polysilicon gate are heavily doped with p-type impurities and connected with metal pads. The body metal contacts are formed by the heavily doped n-type regions of the substrate. When a positive voltage is applied to the gate with respect to the body, holes are pulled towards the upper interface of the gate oxide and electrons are accumulated near the bottom surface of the gate oxide causing reduction in the refractive index of the silicon and causes phase modulation. Since the change in free carrier density is more localized and hence causes high ,polarization dependency. Moreover this structure offers poor modulation depth and few GHz of bandwidth. In addition to that the structure require more interaction length for getting a π phase shift.

Carrier Depletion: The depletion type modulator with p-n structure is shown in figure 1.7. Here the majority carriers are depleting from the pn junction and introducing

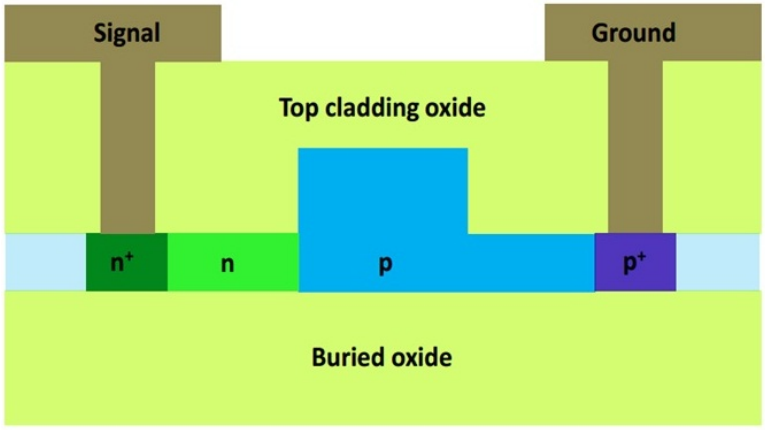

Figure 1.7: Cross-sectional view of p n depletion based modulator in SOI platform [13].

an increase in the refractive index resulting to the phase shift. This model successfully demonstrated for a data rate of 50 Gbps with an extinction ratio of 3.1 dB,and an insertion loss of 7.4 dB. This structure requires an interaction length of 1mm for π phase shift.

Carrier Injection: The Injection type modulator with p-i-n structure is shown in figure 1.8. The structure is showing intrinsic rib waveguide in which a thin region of the top surface of the rib is moderately doped with p-type impurities and the slab which away from the rib side walls are heavily doped with n-type impurities forms a

symmetric p-i-n diode. Heavily doped slab regions act as cathodes and the top surface of the rib acts as anode. When forward bias is applied, carriers are injected towards the active region causing reduction in the refractive index. This results a phase shift for the light passing through it. This configuration is having the following features like high modulation depth or efficiency, requires less interaction length for π phase-shift and lower insertion loss. But for high speed application this configuration is not suitable, because its bandwidth is of the order of few MHz. This is due to the presence of diffusion(storage) capacitance in the forward biased operation.

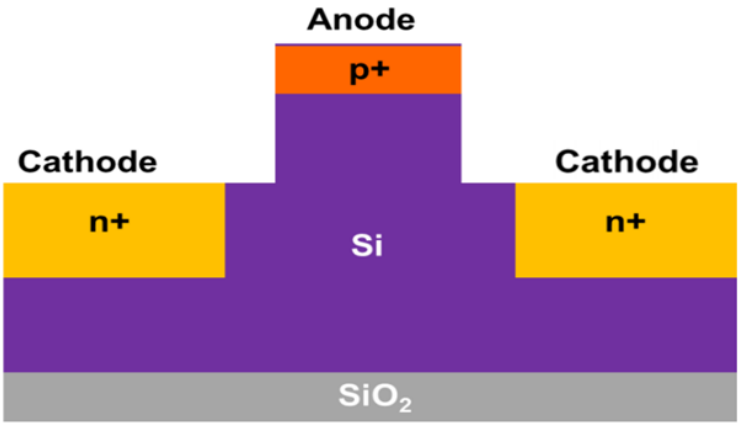

Figure 1.8: Cross-sectional view of p-i-n injection based modulator in SOI platform [14].

1.4 Thermo-optic Effect

Temperature dependent refractive index change of crystalline silicon is $\frac{dn}{dt} = 1.86\times10^{-4}$/K and the thermal conductivity is 163 W/m-K. The increase or decrease in the temperature can cause a change in the refractive index because of the change introducing in the atomic spacing of the material. This will alter the inter band energy state explained by single and double oscillator models[15]. The general structure for thermo optic modulator is shown in figure 1.9. The Nickel chromium(Nicr) and Titanium gold(Ti-Au) are materials having resistivities $1.5\times10^{-6}\Omega m$ and $0.02\times10^{-6}\Omega m$ respectively[17]. These materials are used for providing localized heating over the waveguide region. The main advantage of thermo-optic modulators are they will not introduce additional loss due to absorption, it is efficient too. The main disadvantages are, it is very difficult to lo-

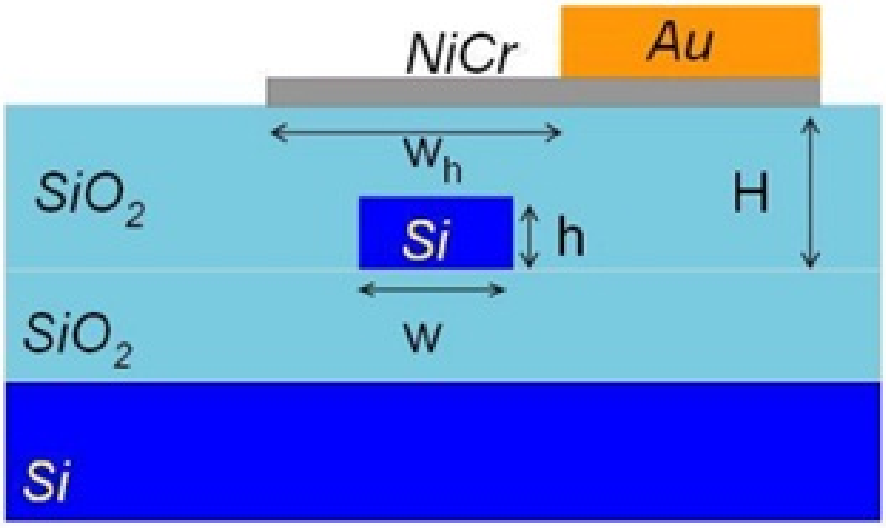

Figure 1.9: Cross sectional view of Thermo-optic modulator in photonic wire dimension with SOI platform [16].

calize the heat because of spreading, heating is slow process. Compared to Si, SiO_2 having very poor thermal conductivity(1.38 W/m-k), this will reduce the efficiency of modulation. Hence this configuration is not suitable for high speed devices.

1.5 Motivation

There are numerous modulators fabricated and demonstrated successfully on SOI platform all over the world. For the past one decade research in this area is progressing considerably. Now a days the fabrication of modulator is CMOS compatible, but the designing is a big challenge. In order to design a modulator we need to analyze the electrical as well as optical characteristics of that device. These analyses are carried out using various commercial simulators, such as T-CAD Medici for electrical characteristics. Which is basically a Poisson's equation solver. Lumerical mode solver is used for optical characteristics by solving Maxwell's equation. Currently there are no efficient and reliable simulators available for solving the electrical as well as optical characteristics of the modulator simultaneously (in a single package). A computation method is already developed in Integrated Optoelectronics laboratory IIT madras related to this issue [25], which can solve the steady state electrical and optical characteristics efficiently for a p-i-n phase modulator. Extention of this work will be useful for solving the

time dependent or transient electrical and optical characteristics of the p-i-n phase modulator. This is vital for designing high-speed modulators. In addition to that study of self heating effect of the modulator is important, because of the thermo - optic properties of silicon which can be utilized for modulation. Moreover the self heating is faster and localized compared to conventional thermo optic modulators[23].

1.6 Research Objective

The objective of the research is to develop a numerical simulation tool to solve simultaneosly the steady state as well as the transient electro-optic and steady state thermo-optic characteristics of waveguide based p-i-n phase-shifter device. The entire thesis work sub-divided as below

(1) Incorporate transient effects in the previously developed mode solver in the lab.

(2) To study thermo-optic effect due to self heating

(3) Validate the computed results with commercial device simulators T-CAD Medici and Lumerical mode solver.

The platform used for computation is Matlab with uniform finite difference technique.

1.7 Thesis Organization

The thesis work contains four chapters. First chapter consists of introduction and survey about modulation mechanisms and the various configurations of modulators has been discussed here. The second chapter discusses the basic principles of modulation, background theory and computation method. Followed by, simulations and results have been discussed in third chapter. In final chapter, summary and outlook of this project has been discussed.

CHAPTER 2

Background Theory and Methodology

This chapter discusses the background theory associated with modulation and the computation algorithm for device simulation. This includes both plasma dispersion and thermo-optic effects.

We know that the equation of plane electromagnetic wave is represented by

$$U(r,t) = U_0 \overline{a} \exp(j(k.r - \omega t + \varphi)) \tag{2.1}$$

where $U(r,t)$ is the plane electromagnetic wave which varies with respect to space as well as time. U_0 is the amplitude of the wave, $\overline{a}$ is representing the polarization of the wave,k is the wave number, r representing the position vector and φ is the phase of the wave. The phase is represented as

$$\varphi = \frac{2\pi}{\lambda} nl \tag{2.2}$$

where λ is the wave length, n is the refractive index of the medium, l is the length at which wave traveled. From the above relations it is clear that if we change the refractive index of the medium the phase can be altered and the modulation is achieved through phase shifting. In section 1.3 the plasma dispersion effect has been explained for phase shifting application. Which is obtained through change in real and imaginary part of refractive index via variation in mobile/free carrier concentration. The Drude model is used to derive an analytical expression for absorption, α. This change in absorption leads to a change in the complex refractive index. The equation (Drude-Lorentz equation), relating the change in free carrier concentration and optical absorption as,

$$\Delta\alpha = \frac{e^3 \lambda_0^2}{4\pi^2 c^3 \epsilon_0 n} \left(\frac{N_e}{\mu_e (m_{ce}^*)^2} + \frac{N_h}{\mu_h (m_{ch}^*)^2} \right) \tag{2.3}$$

and the corresponding equation for change in real part of refractive index ($\Delta\ n$) is,

$$\Delta n = \frac{e^2\lambda_0^2}{8\pi^2 c^2 \epsilon_0 n}(\frac{N_e}{m_{ce}^*} + \frac{N_h}{m_{ch}^*}) \tag{2.4}$$

N_e, N_h are the electron and hole concentrations, μ_e, μ_h are the electron and hole mobilities, m_{ce}^*, m_{ch}^* are the electron and hole effective masses respectively. e is the electron charge, λ_0 is the free space wavelength 1.55μm, ϵ_0 is the free space permittivity and n is the refractive index.

Based on the experimental data, an empirical fit for Δn, $\Delta\alpha$(at λ = 1.55μm) was produced by Soreff and Benette, which was found to be in close agreement with that predicted by the Drude-Lorentz equation (2.3) and (2.4).

$$\Delta n = \Delta n_e + \Delta n_h = -[8.8 \times 10^{-22}\Delta N_e + 8.5 \times 10^{-18}(\Delta N_h)^{0.8}] \tag{2.5}$$

$$\Delta \alpha = \Delta \alpha_e + \Delta \alpha_h = -[8.5 \times 10^{-18}\Delta N_e + 6.0 \times 10^{-18}\Delta N_h] \tag{2.6}$$

where ΔN_e and ΔN_h are the change in electron and hole concentrations respectively. In this simulation the injection mode p-i-n structure has been used for phase - shifting application. The detailed operation of a p-i-n phase modulator has been discussed in section 1.3.

2.1 Background Theory-Electrical Characteristics

The p-i-n phase shifter is a two terminal active device in electrical terminology. The analyses of equilibrium, steady state and transient current(I)-voltage(V) characteristics are being carried out. The key electrical parameters which will determine the performance of the device are potential distribution, electric field, carrier concentration, current density and recombination rate. These parameters are solved using Poisson's and Laplace equations at equilibrium, transport and continuity equations are used for solving the steady state and transient situations. Considering the general structure of the device as shown in the following figure 2.1. In the rib shaped structure the p and n

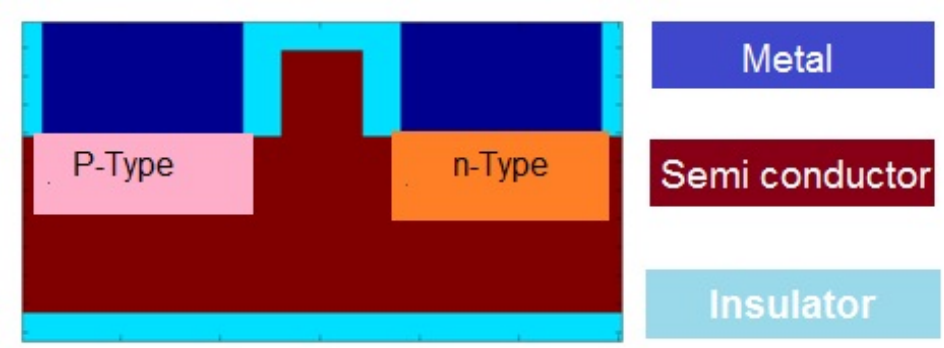

Figure 2.1: p-i-n diode structure with rib waveguide geometry.

type materials are doped both sides of it, The remaining semi conductor region kept as intrinsic forming a p-i-n structure. Different electrical situations are discussed as [19],

Equilibrium: There is no external field applied across the terminal of the device. The Gauss law states that the total electric flux through any closed surface is equal to the total charge enclosed by that surface. For the linear (electric flux density D is linear to the electric field E), homogeneous (ϵ is constant within the structure) and isotropic (D and E have same direction) medium, the Poisson's equation can be written as,

$$\nabla^2 V = -\rho/\epsilon \tag{2.7}$$

If the close surface does not have any charge density , the poisson's equation will become Laplace equation. In 1D, equation 2.7 can be represented as,

$$\frac{d^2V}{dx^2} = -\rho(x)/\epsilon \tag{2.8}$$

The equation is assuming 2-dimensional case and is given by

$$\frac{d^2V}{dx^2} + \frac{d^2V}{dy^2} = \frac{-\rho}{\epsilon} \tag{2.9}$$

The ρ in this equation is the net charge density which is a dependent variable, in this case the variable is electric potential. Hence it is called as non-linear poisson equation. As mentioned earlier for insulator region Laplace equation is used and it is given by

$$\frac{d^2V}{dx^2} = 0 \tag{2.10}$$

For metallic region the potential V is constant. The various input for solving this equations are doping distributions, intrinsic carrier concentrations, thermal voltage v_t and the di-electric constant ϵ. The solution of these equation will give the equilibrium potential, electric field, electron and hole concentrations. This is the initial condition for getting the steady state solutions.

Non-equilibrium: In equilibrium, since the drift is balanced by diffusion for both electrons and holes only poisson's or Laplace equations are sufficient to solve the characteristics. The non equilibrium voltages are applied in terms of steps that are normalized to thermal voltage v_t. Whenever the electric field applied across the diode,it changes the carrier dynamics. Conduction is happening in a semiconductor through Drift(which is due to presence of electric field) and Diffusion(which happens because of concentration gradient). Considering both these effects, here in addition to poisson's and Laplace equations we need to solve **transport** equations

$$J_p(x) = q\mu_p(x)p(x)E(x) - qD_p(x)\frac{dp(x)}{dx} \tag{2.11}$$

$$J_p(x) = q\mu_p(x)p(x)E(x) - qD_p(x)\frac{dp(x)}{dx} \tag{2.12}$$

and **continuity** or **rate** equations

Rate of carrier buildup = Net generation rate - Net rate of carriers leaving
Writing in derivative form,

$$\frac{\partial p}{\partial t} = g - \frac{1}{q}\frac{\partial J_p}{\partial x} \tag{2.13}$$

$$\frac{\partial n}{\partial t} = g + \frac{1}{q}\frac{\partial J_n}{\partial x} \tag{2.14}$$

For steady state the time dependent part is zero and is given by

$$\frac{\partial p}{\partial t} = 0 \tag{2.15}$$

$$\frac{\partial n}{\partial t} = 0 \tag{2.16}$$

where q is electron charge and is = 1.6 $\times 10^{-19} Coloumb$. J_p, J_n are the current density of hole and electron respectively. μ_p, μ_n are the mobility of hole and electron. E is the electric field. p, n are the hole and electron concentrations. D_p, D_n are the diffusion constants and can be related to mobility with following Einstein relation.

$$\begin{aligned} D_p &= \mu_p \times V_t \\ D_n &= \mu_n \times V_t \end{aligned} \tag{2.17}$$

where V_t is the thermal voltage and = $kT/q = 0.026eV$ at room temperature and x is the distance from anode. where $g = -U$ is the generation-recombination rate of carriers The total current density

$$J(x) = J_p(x) + J_n(x) \tag{2.18}$$

Transient: In transient case the time dependent part of continuity equations are non zero. Fixing an operating point(bias point) is required to carry out the transient analysis.

2.2 Computation Algorithm-General approach

For solving all the previous equations we need to use some numerical method. This is because we are assuming the carrier flow is two dimensional and it cannot be solved analytically. The numerical method is uniform finite difference scheme. This uses central difference method for discretization. In which the equations are solved using **Scharfetter-Gummel**[18] discretization scheme. This method solves the coupled equations in terms of decoupled way. The Poisson's/Laplace equations, Transport and continuity equations are coupled equations. In this method at the equilibrium only the Poisson's/Laplace equations are solved. Since the current is equal to zero at equilibrium (drift balances diffusion) transport and continuity equations are not solving. This makes the convergence of the solutions faster. But at higher bias the dependence between the equations is more so this method generally not suitable at higher bias point. The various

assumptions taken for the computation are

1.Boltzman approximation is valid for the energy states

2.Temperature is at 300K(For electrical characteristics)

3.At 300K complete ionization is taking place

4.Carrier flow is 2-dimensional

5.Surface states are absent

The detailed algorithm for the discretization is described in the first phase of the project "Numerical Analysis of Integrated Optical PIN Phase Modulator"[25]. Besides, which explains how the optical characteristics are solved. The following flow chart represents the procedure or algorithm for solving electro-optic characteristics of p-i-n phase shifter.

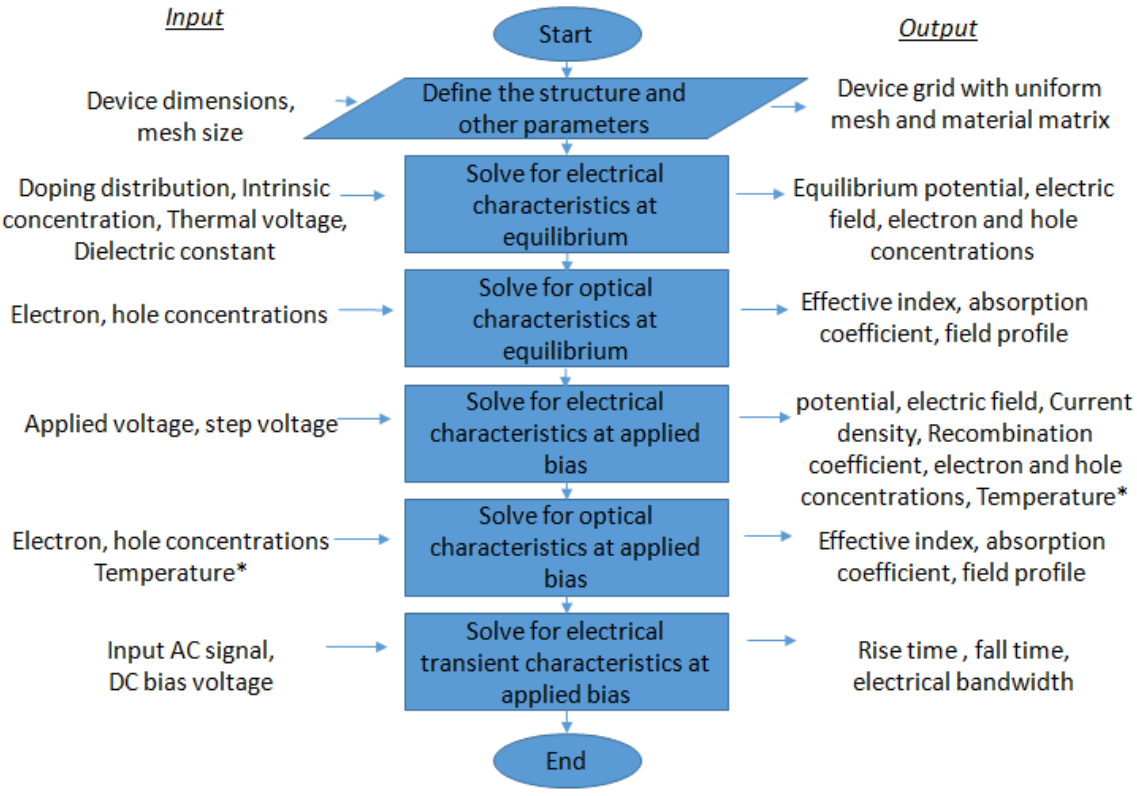

Figure 2.2: Computation procedure for Electro-optic characteristics

The generation-recombination mechanism and implementation of the thermo-optic effect will be discussing in the coming sections.

2.3 Displacement current

The total current density is a combination of both conduction current and displacement current.This is given by

$$J_{total} = J_{conduction} + \varepsilon \frac{\partial E}{\partial T} \tag{2.19}$$

Here $\varepsilon \frac{\partial E}{\partial T}$ represents the displacement current. Under steady state case the time dependent part is zero. For transient case the displacement current is playing a role. In case of reverse bias operation the conduction current is very small at the same time displacement current will play a major role. In case of forward bias it is observed that when we increase the bias voltage the effect of displacement current is decreasing. Because the conduction current is increasing and the rate of change of electric field becomes negligible. Since the computation is carried out in forward bias the displacement current part is not considered in this case.

2.4 Generation and recombination

Generation and recombination are the creation and annihilation of electron-hole pairs respectively. In a forward biased diode the recombination is dominating and the different recombination mechanisms are

Band to band recombination: It is a direct recombination mechanism in which electron falls directly from the occupied state in the conduction band to the empty state in the valence band associated with a hole[20]. For direct band gap materials this is a radiative recombination,for indirect bandgap materials this is a phonon(lattice vibrations) assisted recombination. Since silicon is an indirect band gap material this recombination is absent here.

Shockley Read Hall recombination: This is a trap assisted recombination, in which the electron falls in to trap caused due to the presence of foreign atom or structural defect. The electron occupying in a trap can fall in to empty state of the valence band and complete the recombination process or within the trap itself both electron and hole

can annihilate each other. Hence this type of recombination can happen in two ways.

Auger recombination: This involves three particle the annihilation of one electron-hole pair will creates another electron which is pushed in to the higher energy state of the conduction-band.

The different recombination mechanisms are shown in the following figure2.3

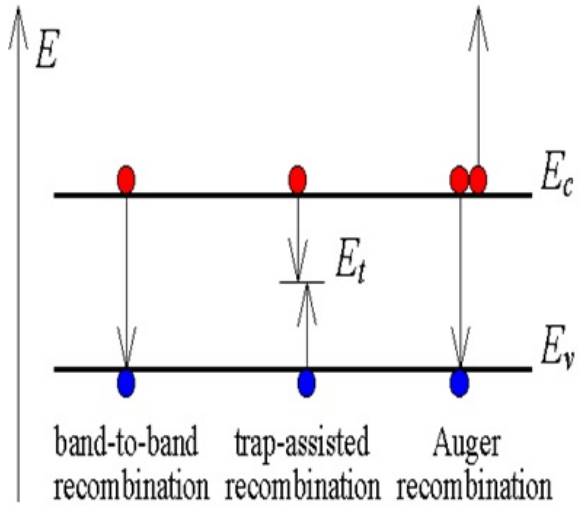

Figure 2.3: Recombination Mechanisms in semi conductor. The different energy state - conduction band minimum E_c, valence band maximumE_v, trap Energy level E_t

2.5 Implementation of temperature effects

As the plasma dispersion effect dominated in silicon, the thermo-optic effect in silicon cannot be ignored and implementation of this effect in simulation will be helpful for getting the results in a more realistic way. As far as the device is concerned the heating effect can be of two types

1.External contact resistance

2.Internal series resistance

In this package we are considering the self heating(due to internal series resistance) which is a bulk property. Implementation of contact resistance requires 3-D assumption that cannot be incorporated here.

2.6 Heat Transfer

Heat transfer is a physical process which has a direction as well as magnitude. The total heat transfer mechanism can be divided as

Conduction: It is the energy transport due to molecular motion and interaction. This mainly happening in solids due to molecular vibration.

Convection: It is the heat transfer due to bulk fluid motion.

Radiation: It is due to the emission of electro magnetic waves or photons from the surface or volume.This process does not require a medium or it can happen in vacuum also.

As far as silicon is concerned it is crystalline solid and the heat transfer is through conduction only. The heat transfer mechanism can be explained by Fourier law of heat conduction[21].

Consider the following fig 2.4 in which the general flow of heat energy is represented as where Q is the heat source or sink in W/m^3. G is the generation rate inside

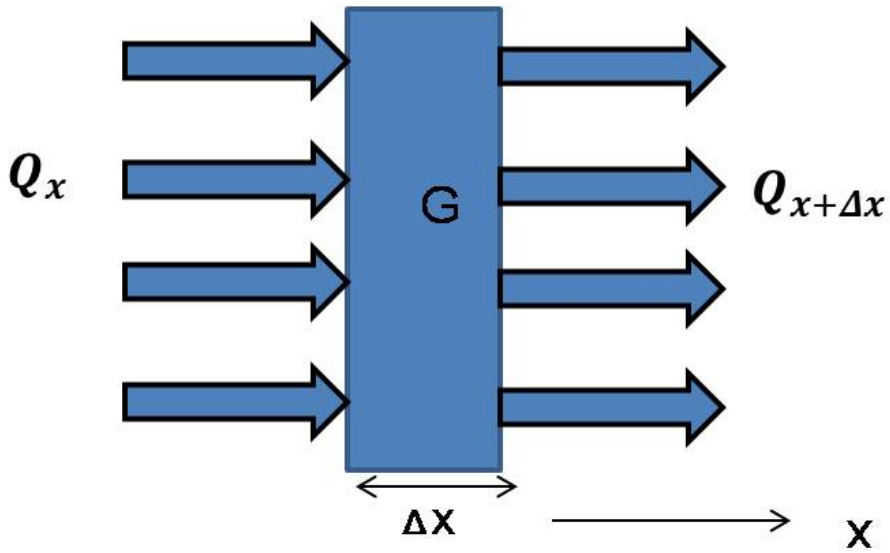

Figure 2.4: One dimensional Heat flow

the element. Connecting all the parameters the rate equation can be written as

$$Q_x - Q_{x+\Delta x} + G = \frac{\Delta E}{\Delta t} \tag{2.20}$$

Where the right hand side of the above equation represents the rate of change of energy content of the element. Where

$$\Delta E = \Delta E_t - \Delta E_{t+\Delta t} \tag{2.21}$$

$$\Delta E_t - \Delta E_{t+\Delta t} = mC(T_{t+\Delta t} - T_t) \tag{2.22}$$

where **m** and **C** are the mass and the specific heat capacity of the material respectively. where

$$mass = density \times volume \tag{2.23}$$

$$m = \rho_v A \Delta x \tag{2.24}$$

where the ρ_v is the density of the material, AΔx is the volume. The generation **G** can be represented as

$$G = gA\Delta x \tag{2.25}$$

Where **g** is the generation per unit volume, thus combining equations 2.20 - 2.24 it is clear that

$$Q_x - Q_{x+\Delta x} + gA\Delta x = \rho_v C A \Delta x \frac{(T_{t+\Delta t} - T_t)}{\Delta t} \tag{2.26}$$

If the eq - 2.26 completely dividing by AΔx and is given by

$$\frac{Q_x - Q_{x+\Delta x}}{A\Delta x} + g = \rho_v C \frac{(T_{t+\Delta t} - T_t)}{\Delta t} \tag{2.27}$$

Taking the limits $\Delta x \longrightarrow 0$ and $\Delta t \longrightarrow 0$ for the above equation and it results as

$$\rho_v C \frac{\partial T}{\partial t} = Q + k\nabla^2 T \tag{2.28}$$

where k is given as the thermal conductivity W/m-k. In steady state condition the equation 2.28 can be written as

$$Q + k\nabla^2 T = 0 \tag{2.29}$$

The above equation is general Fourier heat conduction equation. Where T is the temperature which can be solved analytically. Now the general analytical solution will be of the form

$$T = \frac{-Qx^2}{2k} + C_1 x + C_2 \tag{2.30}$$

The Q can be calculated from the resistivity and current density in the material.Now the boundary condition will be like wherever $x = 0$ implies the current density is zero , the temperature T is a constant and it is equal to 300K. Since the current flow is two dimensional the Fourier heat conduction equation can be solved accordingly. Q can get using the joule heating model where Q is proportional to $J^2\rho$

Where J is the current density and ρ is the resistivity of the material. This is called the Joule heating model, where the resistivity ρ given as

$$\rho = \frac{1}{q(n\mu_n + p\mu_p)} \tag{2.31}$$

the solution for the current density can get from the transport and continuity equation as mentioned in previous section. Since we have the space dependent carrier concentration from Poisson's equation, the resistivity can get from the eq.2.31. The same discretization procedure is used for calculating J as well as ρ. Consider the figure 2.5

Which will give the space dependent resistivity and current density. The details are

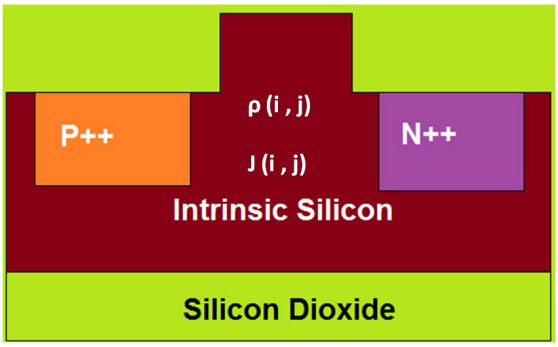

Figure 2.5: p i n structure with space dependent resistivity ρ and current density J,these are the parameters required for calculating the self heating.

given in the previous flow chart (figure 2.2). The detailed calculation procedure give as

$$Q = J^2\rho \tag{2.32}$$

From discretized format we can get J as

$$J = \sqrt{J_x(i,j)^2 + J_y(i,j)^2} \tag{2.33}$$

where i,j are mesh variables. Since current flow is two dimensional J_x and J_y are current densities along x and y directions respectively. From the equations 2.29 and 2.30 with appropriate boundary conditions like when $x, y = 0, 1 \longrightarrow T = 300K$ will give

$$C_2 = 300K, C_1 = \frac{Q}{k}x + \frac{Q}{k}y \tag{2.34}$$

Now back calculating T from 2.30 will give

$$T = \frac{Q}{2k}x^2 + \frac{Q}{2k}y^2 \tag{2.35}$$

From 2.31 - 2.35 the final relation can be written as

$$T = \sqrt{(J_x^2(i,j)x^2)^2 + (J_y^2(i,j)y^2)^2} \times \frac{\rho}{2k} \tag{2.36}$$

The expression 2.30 is used for getting the steady state temperature distribution. Using this information the effective refractive index is calculated.

CHAPTER 3

Results and Discussion

This chapter explains the simulations results of rib waveguide geometry at different arbitrary dimensions(Large cross section to photonic wire rib waveguides) for injection mode operation with p-i-n structure. Three different dimensions have been taken for computation and they were compared with standard simulation results as well as experimental results. Here the different results explained as

3.1 Reduced cross sectional rib waveguide

The reduced cross section indicates the device layer thickness around $2\mu m$. Using this dimension the computation algorithm is explained. First of all the waveguide should be single moded for getting a dispersion free operation. The following plot represents the critical parameters which will determine the single mode operation of the device and it is given as in figure 3.1. Here **H** is the device layer thickness,**h** is the slab height and**W** is

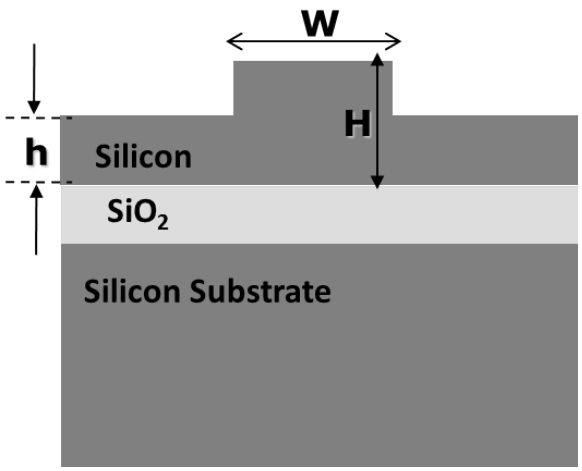

Figure 3.1: Rib waveguide geometry with parameters.

the rib width. By varying any one of the parameter keeping the other two constant will give the appropriate singlemode condition. The next plot showing the region where

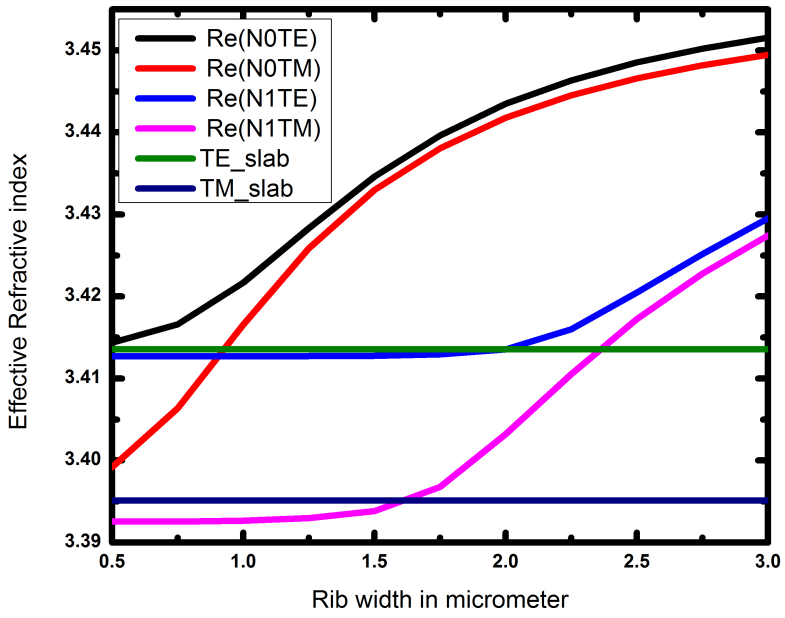

Figure 3.2: Single mode waveguide designing using the effective refractive indices of slab region TE slab and TM slab as well as the rib region with effective refractive indices of fundamental modes N0TE,N0TM and first higher order mode N1TE and N1TM.

this particular geometry works as single mode waveguide. The parameters **H** and **h** kept constant.The rib width **W** is varied from $0.5\mu m$ to $3\mu m$ with keeping H as $2.0\mu m$ and h as $1\mu m$. From the above plot it is clear that The modes whichever having the effective index more than slab effective indices that particular mode will be guided. The fundamental modes transverse electric(N0TE) and transverse magnetic(N0TM) modes will be guiding for all the possible values of W from $0.5\mu m$ to $3\mu m$. In the figure the higher order TE mode N1TE will be a guided mode when W is more than $1.9\mu m$ and TM mode N1TM will be guided when the width is more than 1.6 μm. Once if we know the single mode dimension for rib waveguide, we can define the doping parameters like junction depth, concentration profile etc.

3.1.1 P-I-N Structure with $2\mu m$ SOI

The silicon on insulator will give better confinement and this structure is CMOS compatible as well. The different doping concentration defined for both are p-type and

n-type are 10^{19} cm^{-3}. This will give a better ohmic contact. The intrinsic carrier concentration is taken as 2.5×10^{12} cm^{-3}. Since the doping profile is constant this will make a uniform current flow in between p and n.The junction depth kept 0.5 μm. The doping window is $5\mu m$. Making sure that the mode profile is not interacting with doped regions, such a way that the loss can be minimized.

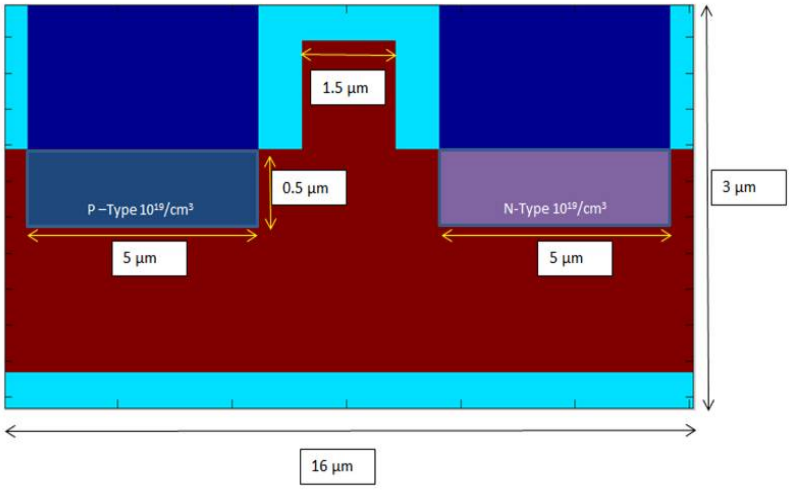

Figure 3.3: Simulation structure for reduced cross section rib waveguide with doping parameters.

The thickness of buried oxide layer is $1\mu m$.

3.1.2 Equilibrium and Steady state Electrical characteristics

The various equilibrium and steady state results are given as follows.

Equilibrium : The potential distribution at equilibrium along x-axis(indicated as black line in the right part of figure 3.4) is shown. For a doping concentration of 10^{19} cm^{-3} the built in potential is 1.05 Volts.

Appliedbias/Steadystate : When 1 V external bias is applied at the anode, the potential distribution along the same line as before is given in figure 3.5. The potential dropped mostly at the intrinsic region, and the potential drop at doped region is negligible. The total drop at these regions can be modeled in terms of series resistance and this will be discussed detailed way in section 3.2.1

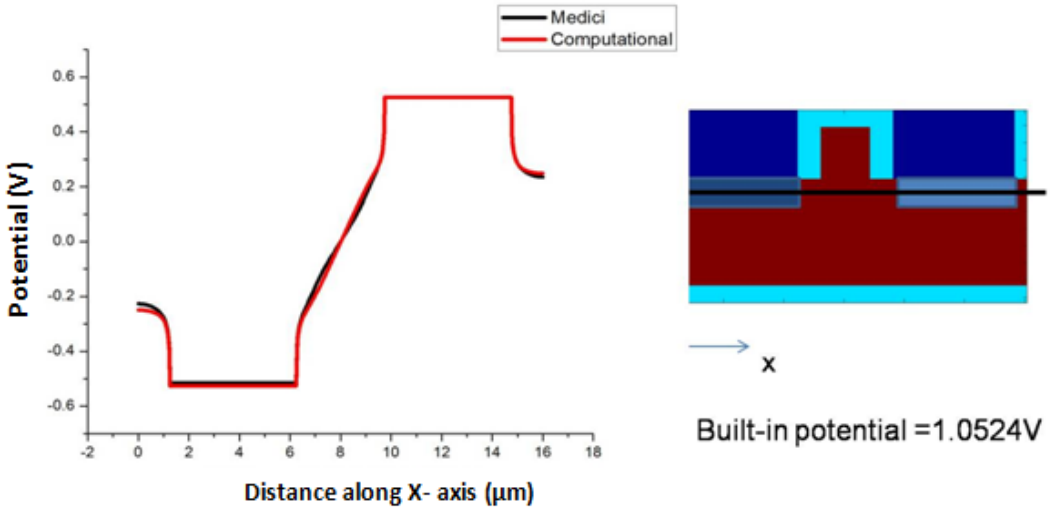

Figure 3.4: One dimensional plot of potential distribution at equilibrium along the structure in x-direction.

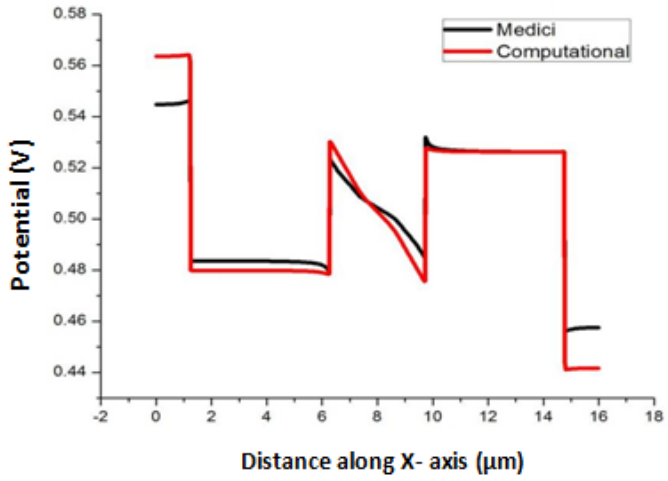

Figure 3.5: Potential distribution at 1V applied bias.

3.1.3 Steady state Optical characteristics

The concentration profile which derived from both zero bias and applied bias will be used to find the steady state optical characteristics. The change in refractive index and absorption can be found using formula 2.5 and 2.6 and this is used to calculate the effective index using a semi-vectorial mode solver [25]. Using the effective index we can calculate the interaction length required for calculating the π phase shift. The detailed calculation as follows

$$L\pi = \frac{\lambda}{2(Neff_0 - Neff_1)} \tag{3.1}$$

The following figure represents the different values of effective indices at zero bias and one volt. The simulated results using medici that imported to lumerical is compared here with computed results.

Neff (Imported from Medici)		Neff(Directly from Matlab code)	
TE0V	3.436943	TE0V	3.435701
TE1V	3.432680	TE1V	3.431601
TM0V	3.434926	TM0V	3.433903
TM1V	3.430653	TM1V	3.429801

Lπ (Imported from Medici in to Lumerical Mode solver) (Microns)		Lπ (Numerical Computation) (Microns)	
TE	TM	TE	TM
181.790	181.370	189.024	188.932

Figure 3.6: Steady state parameters for L_π calculation using fundamental mode refractive indices at equilibrium TE0V,TM0V and at applied bias TE1V,TM1V.

The figure of merits are 0.189V-mm for TE and 0.188V-mm for TM respectively. TE0V,TM0V and TM0V,TM1V are the effective indices for TE and TM at different bias points.

3.1.4 Transient Electrical characteristics

The transient elecrical characteristics is very important for finding the electrical band width which will determine the speed of operation of the device. The detailed procedure for transient analysis was explained in section 2.1. Here the pulse with 100ns duration applied with a magnitude of 30mV, keeping the dc biasing point at 1V. The rise time and fall time which obtained are 4.8ns and 0.12ns respectively. The result is verified using T-CAD Medici and accordingly the rise and fall time are 4.86ns and 0.73ns respectively. The detailed discussion of transient effect is given in the section 3.2.2.

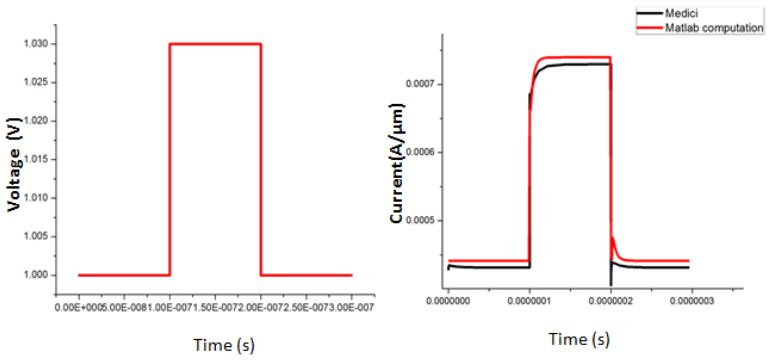

Figure 3.7: Electrical characteristics with transient input voltage and current response.

3.1.5 Transient Optical characteristics

The various time dependent optical characteristics were computed. The parameters are absorption and effective refractive index. The assumption taken here is, there will not be any delay for the changes in optical parameters with respect to time dependent change in electrical parameters. This shows the time dependent refractive index change and

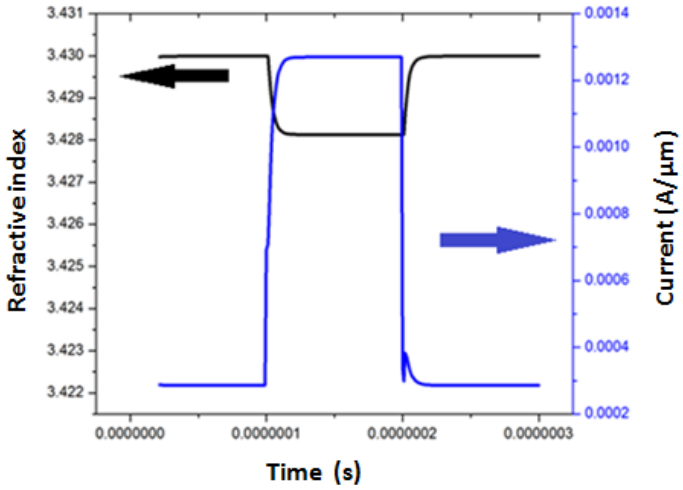

Figure 3.8: Time dependent refractive index variation with current.

transient current response is given as well. The next figure shows the time dependent absorption characteristics. This type of studies will help to estimate the pulse amplitude such a way that the absorption should not increase much.

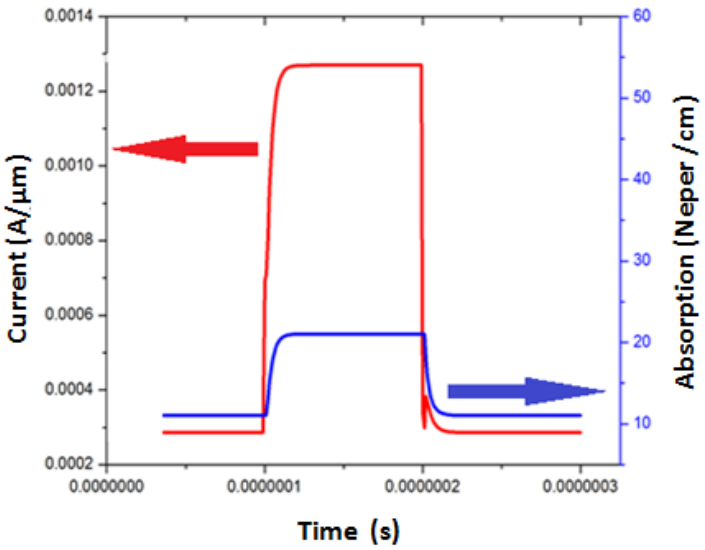

Figure 3.9: Time dependent absorption variation with current.

3.2 Large cross sectional rib waveguide

The Large cross section indicates the device layer thickness around 5μm. In this particular section the computed results are compared with some of the experimental results. There are number of advantages for the large cross section rib structure like

(i) Easy to fabricate compared to other dimensions

(ii) Easy to couple light from fiber because of index-matching.

(iii)Polarization independent

The following figure will show the dimensions for the large cross section p-i-n phase shifter. This particular dimension is single moded for the wavelength 1.55 μm. The diffusion doping is done and the doping concentrations for both p and n type are 5×10^{19} cm^{-3}. The background concentration is 2.5×10^{19} cm^{-3}. The junction depth are keeping 1.0 μm such that the maximum current density will be exactly overlapping with maximum field of the optical mode[24]. This will give optimized interaction length required for π phase shift.

The following sketch 3.11 is the top view for the fabricated device. The conventional way of simulation gave L_π around 230 μm with the applied bias of 1V for both TE and TM. The numerical computation using Matlab gives L_π around 204 μm.

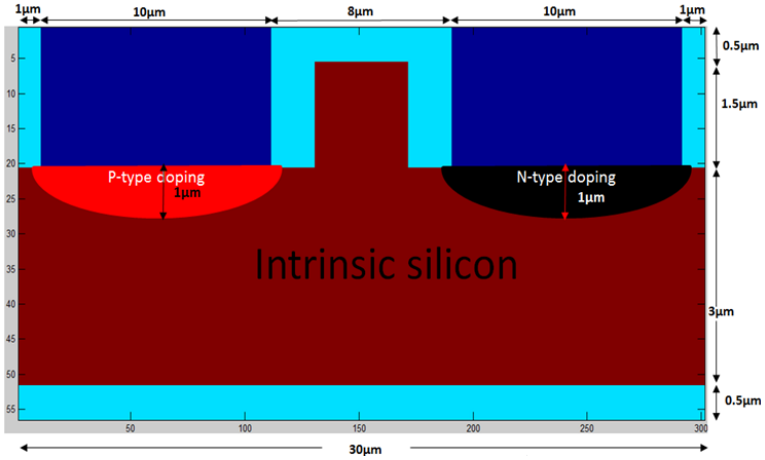

Figure 3.10: Large cross section rib structure with diffusion doping.

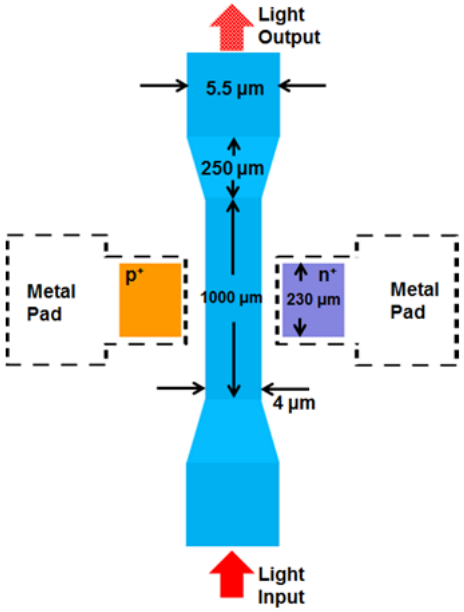

Figure 3.11: The variable optical attenuator on Large cross section.

3.2.1 Computed results for Large cross sectional device

I-V Characteristics: The following figure shows the voltage-current characteristics for this device. There are some important parameters which can be extracted from the I-V characteristics, such as **Series resistance**,**Diffusion capacitance**. They are very important parameters as far as the high-speed operations are concerned. This will be contributed to the total RC time delay.

Series resistance: At higher injection the effect of series resistance is dominating because of the bulk drop. At lower and moderate injection case the drop due to series

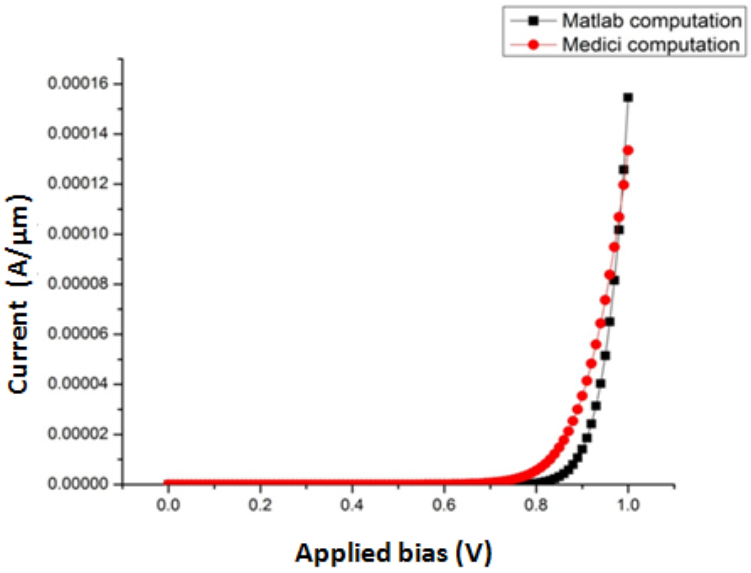

Figure 3.12: I V characteristics of the diode.

resistance is decreasing because of the lower current. As the current increases potential drop increases. The extraction method[22] is followed as, For the two voltage points in the figure 3.13, V1 and V2 the current-voltage relation is given by

$$I = I_0(e^{(\frac{V2}{V_t}} - 1) \tag{3.2}$$

$$I = I_0(e^{(\frac{V1-IR}{V_t}} - 1) \tag{3.3}$$

Where the equation 3.2 represents the ideal diode equation where as 3.3 represents the non-ideal situation because of series resistance. Where **R** is the series resistance, I_0 is the reverse saturation current. I is the current at a particular voltage, v_t is the thermal voltage. Equating 3.2 and 3.3 given as

$$R = \frac{V2 - V1}{I} \tag{3.4}$$

The series resistance that calculated through this way is 1.3Ω at 1V.

Trans-resistance: This is a small signal resistance as shown in the figure 3.15. This

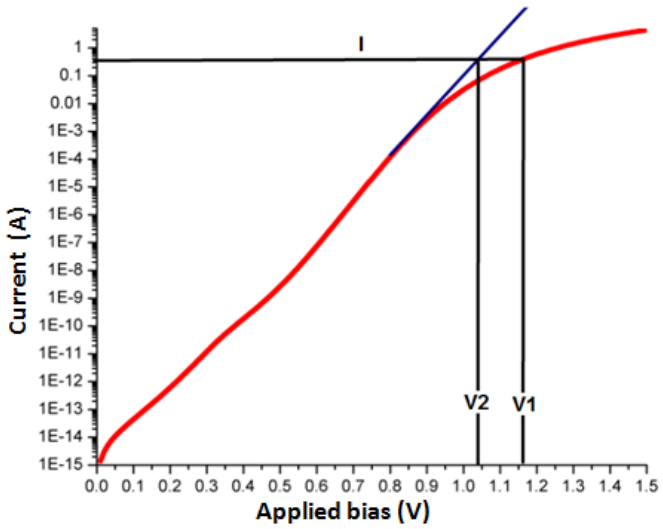

Figure 3.13: Series resistance Extraction.

will ensure a default path for the dc current. The trans resistance r_t given as

$$r_t = \frac{v_t}{I} \tag{3.5}$$

The computed value is 0.723Ω at 1V.

Diffusion capacitance: This is otherwise called as storage capacitance. This is due to the minority charge injected from both the p and n side of the diode. In p n junction the following figure shows the excess carriers. In case of p-i-n diode the intrinsic region will be almost depleted. As in p-n junction diode at certain applied bias,minority carrier will be stored. This will introduce diffusion capacitance. The analytical equation for calculating the diffusion capacitance is given by

$$C_{diffusion} = g_p \tau p + g_n \tau n \tag{3.6}$$

$$g_p = \frac{I_p}{v_t}, g_n = \frac{I_n}{v_t} \tag{3.7}$$

where I_n and I_p are electron and hole current respectively. τn and τp are electron , hole lifetime respectively. In case of short diodes,where the diffusion length is more than the transition region, the diffusion process will not take place. Instead they will transit, in this case the life-time in equation 3.6 can be replaced by transit-time τ_t. This

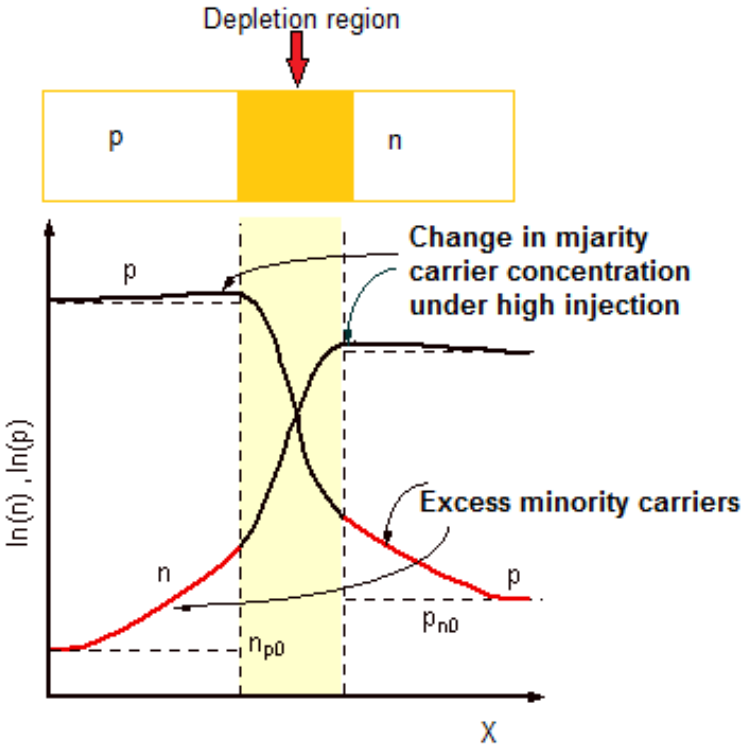

Figure 3.14: Carrier concentration variation in a pn Junction.

will reduce the stored capacitance, by transiting the carriers. In case of forward bias the **depletion capacitance** is very small compared to **diffusion capacitance** because of the less displacement current. Combining the parameters-R,r_t,C diffusion and C depletion the small signal equivalent circuit can be modeled as

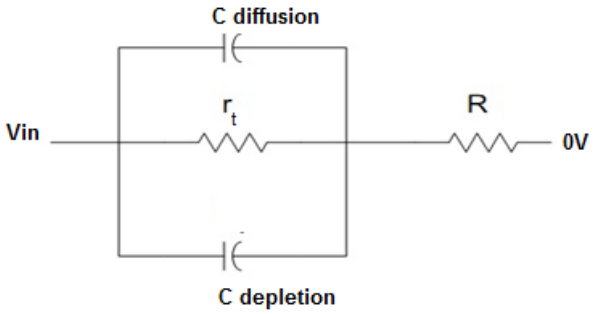

Figure 3.15: Small signal equivalent circuit of a diode.

Numerical way of calculating capacitance: The numerical way of calculating the

capacitance can be explained as

$$C = \frac{\Delta Q}{\Delta V} \tag{3.8}$$

$$\Delta Q = \frac{\Delta I \times \Delta t}{\Delta v} \tag{3.9}$$

Using this relationship the ΔQ is the area under the curve for a response current. The response current can get by applying a small signal input pulse. The following figure shows the current response of with the application of 4mv-200ns pulsed voltage signal, keeping the biasing point at 1V. The diffusion capacitance extracted using this method

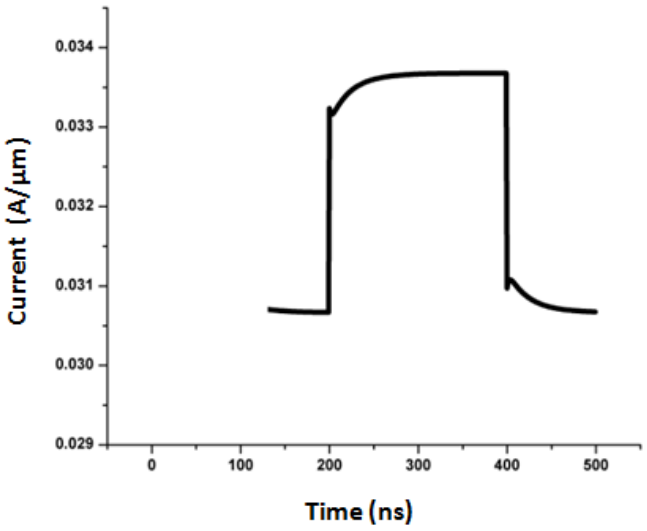

Figure 3.16: Numerical way of calculating diffusion capacitance by area under the curve.

is 122.2nf/μm. For analytical expression the value is 131.6/μm. With the values of $\tau p = \tau n = 10^{-7} ns$.

3.2.2 Transient Analysis

In case of Large cross section rib wave guide the operation speed will be low because the transit time required for the carriers from one electrode to the other is more compared to the reduced cross section rib waveguide.

The figure represents transient response for the device with an input pulse keeping biasing point at 1V.

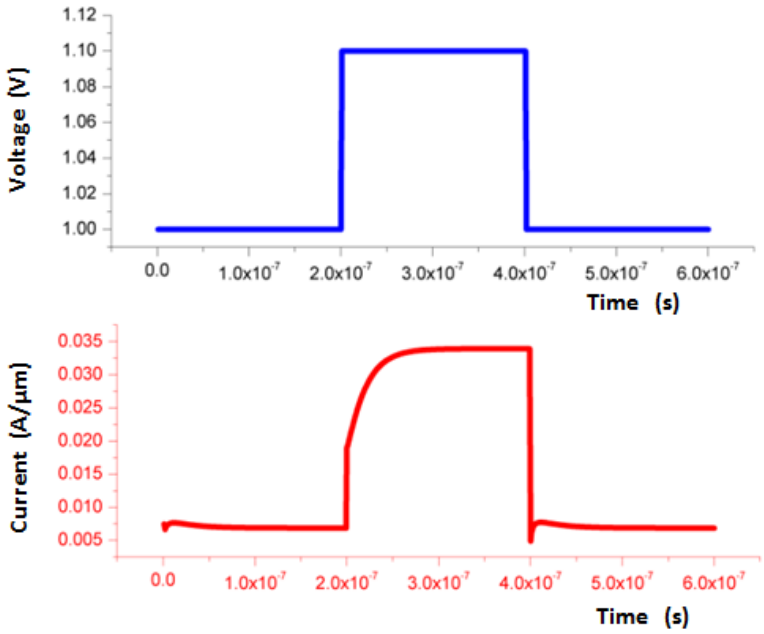

Figure 3.17: Transient response for large cross section rib waveguide based p-i-n diode.

The equivalent circuit model will give a very good idea about the transient dependence of different parameters. The series resistance R and diffusion capacitance **C** plays major role in determining the RC time constant of the device. For transient analysis we need to fix a bias point, if the bias point is very small (0-0.5V) forward bias the resistance offered by device will be more and depletion and diffusion capacitance will play a role in the time constant of the device. If the forward bias voltage is too-high that will decrease the series resistance R, because more carriers will be injected into the intrinsic region this will reduce the value R. But at higher bias point the diffusion capacitance value will be high becuase, the current at higher injection will be more and it is directly proportonal to diffusion capacitance. In otherwords the storing charges (minority carriers) will be more in case of higher injection. This means diffusion capacitance is high. Thus from these observations it is clear that there should be some trade-off for choosing dc bias point. Moderate level bias is preferable. The R does not include the contact resistance.

3.2.3 Effective refractive index and absorption characteristics

The effective refractive index and absorption characteristics for TE mode is given below. The effective refractive index decreases and absorption increases with the applied bias. The absorption characteristics of TE polarization compared with standard simula-

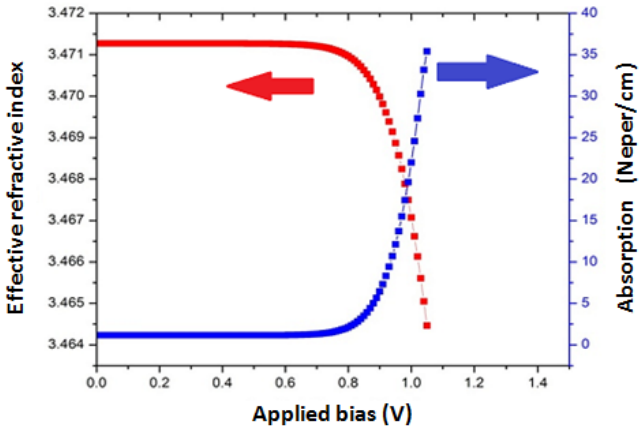

Figure 3.18: Effective refractive index and absorption characteristics with forward bias.

tion results and experimental results and given in figure 3.19. The experimental curve includes the waveguide loss also.

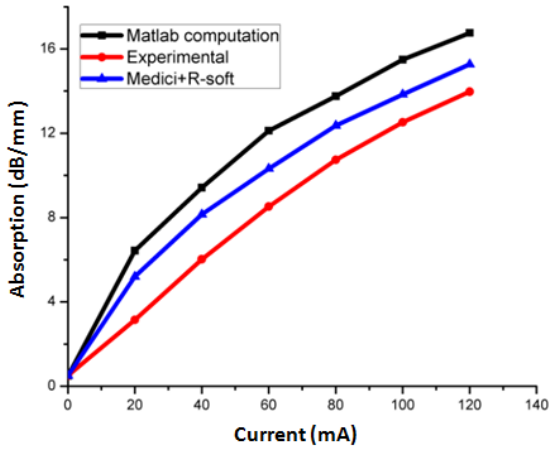

Figure 3.19: Variation of Absorption with current for TE polarization.

The absorption results of TM polarization are then compared with experimental result including waveguide loss,this is in figure 3.20.

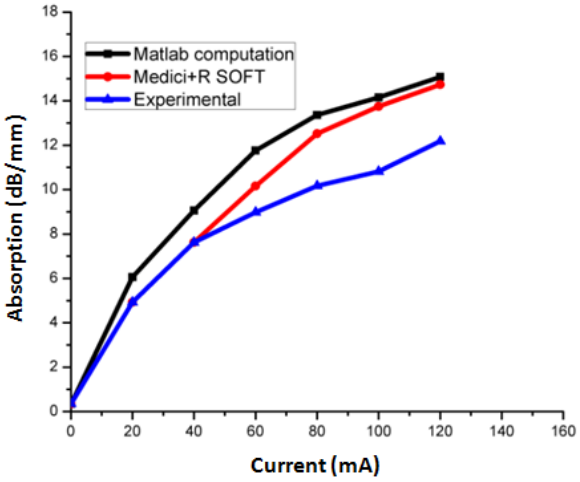

Figure 3.20: Variation of absorption with current for TM polarization.

3.2.4 Thermo-optic characteristics

The thermo-optic properties of silicon were explained detail in section 2.5. The self heating mechanism due to joule heating was also discussed. Here the computed results were compared with experimental results. Consider the following figure 3.21,

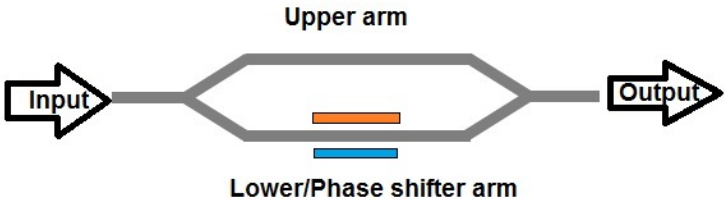

Figure 3.21: Mach-Zehnder modulator.

where the Mach-Zehnder modulator configuration is used for the analysis. The detailed analyses of MZI is given as,

The electric field at the input can be written as,

$$E_{in} = E_p e^{j\omega t} \tag{3.10}$$

$$E = \frac{E_{in}}{\sqrt{2}} \tag{3.11}$$

Let E_p be the peak electric field at the input port, α and $\alpha+\Delta\alpha$, β and $\beta+\Delta\beta$ be the attenution, phaseshift constants of reference and modulating arms of MZI respectively. The electric field at any point along the upper arm (E_{up}) may be written as,

$$E_{up} = \frac{E_p}{\sqrt{2}} e^{(-\alpha+j\beta)z+j\omega t} \tag{3.12}$$

the electric field for the modulating (E_{mod}) arm (at any point beyond the p-i-n waveguide) is written as,

$$E_{mod} = \frac{E_p}{\sqrt{2}} e^{(-\alpha+j\beta)z+(-\Delta\alpha+j\Delta\beta)l+j\omega t} \tag{3.13}$$

where l is the length of the p-i-n diode / waveguide. The total electric field at the output eof the MZI is the sum of electric field from thee upper and lower phase shifter arms.

$$E_{out} = E_{up} + E_{mod} \tag{3.14}$$

$$E_{out} = E_{up}\{1 + e^{(-\Delta\alpha+j\Delta\beta)l}\} \tag{3.15}$$

The intensity of light at the output port (S_{out}) of MZI can be written as

$$S_{out} = E_{out}E^*_{out} \tag{3.16}$$

$$S_{out} = E_{up}E^*_{up}\{1 + e^{(-\Delta\alpha+j\Delta\beta)l}\}\{1 + e^{(-\Delta\alpha-j\Delta\beta)l}\} \tag{3.17}$$

$$S_{out} = \frac{|E_p|^2}{2} e^{-2\alpha z} \{1 + e^{(-\Delta\alpha - j\Delta\beta)l} + e^{(-\Delta\alpha + j\Delta\beta)l} + e^{-2\Delta\alpha l}\} \tag{3.18}$$

$$S_{out} = \frac{|E_p|^2}{2} \{cosh(\Delta\alpha l) + cos(\Delta\beta l)\} e^{(-2\alpha z - \Delta\alpha l)} \tag{3.19}$$

$$\frac{S_{out}}{S_{in}} = \frac{1}{2} \{cosh(\Delta\alpha l) + cos(\Delta\beta l)\} e^{(-2\alpha z - \Delta\alpha l)} \tag{3.20}$$

Using the equation 3.20, consider the following figure 3.22, which shows the experimental results which include the plasma dispersion and thermo-optic effect, the figure 3.22 shows the simulation considering only the plasma dispersion effect.

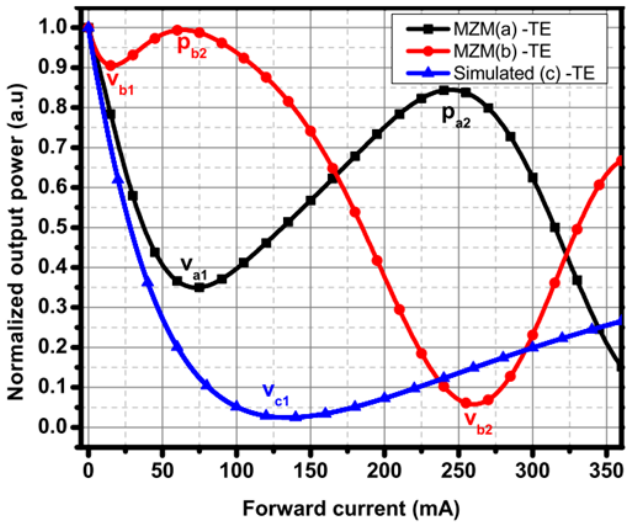

Figure 3.22: Power Characteristics of a Mach-Zehnder modulator with experimental result including plasma dispersion and thermo optic effect,simulations by considering only plasma dispersion effect[24].

Here two curves were experimental and the other one is simulated. An effort was made in our computation to implement the thermo-optic effect due to self heating of the device. The following assumptions were taken in to account for this as

i)Heating due to contact resistance is not considered: To incorporate this the 3-

dimensional simulation package is required.

ii)The increment in the temperature is not accounted for the electrical characteristics: The thermal voltage, other temperature dependent parameter changes are negligible for the small increment in temperature.

The figure 3.23 represents the changes in effective refractive index due to thermo-optic effect which is really opposite to the effect due to plasma dispersion. This is indicated in the figure.

The injection of the carrier decreases the effective refractive index. Where as temperature increment increases the effective refractive index. In the figure 3.23 the changes in refractive index plotted with voltage and after 1.2 V the thermo-optic effect dominated over plasma dispersion effect.

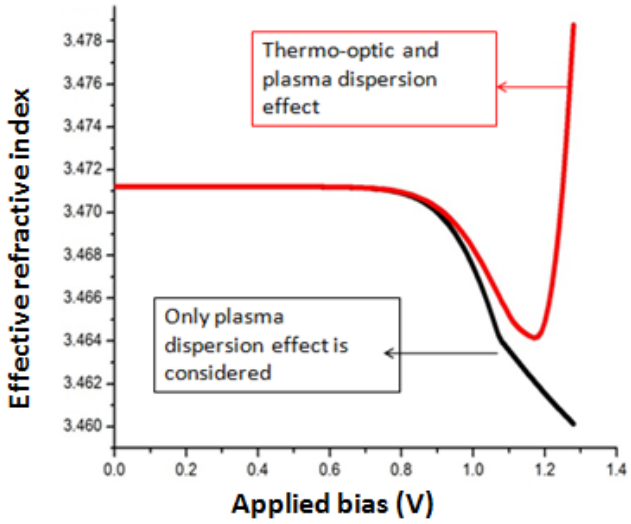

Figure 3.23: Effective refractive index variation for TE mode.

Using the equation 3.20, where including the thermo optic refractive index change the normalized power for structure is given in 3.24. Here the current required for visualizing the thermo optic effect is much larger because the contact resistance is not considered. The current required to visualize the thermo-optic dominating effect is around 800 mA but in reality this is very less and around 50mA, because of the contact resistance. Ideally the absorption is idependent of thermo optic effect. This type of thermo-optic modeling is very good for designing low loss modulators. The reverse bias will be good for this purpose because carrier depletion will reduce the absorption

and effectively increases the refractive index as in case of thermo-optic modulation. The figure 3.25 represents a depletion type modulator incorporating thermo-optic effect.

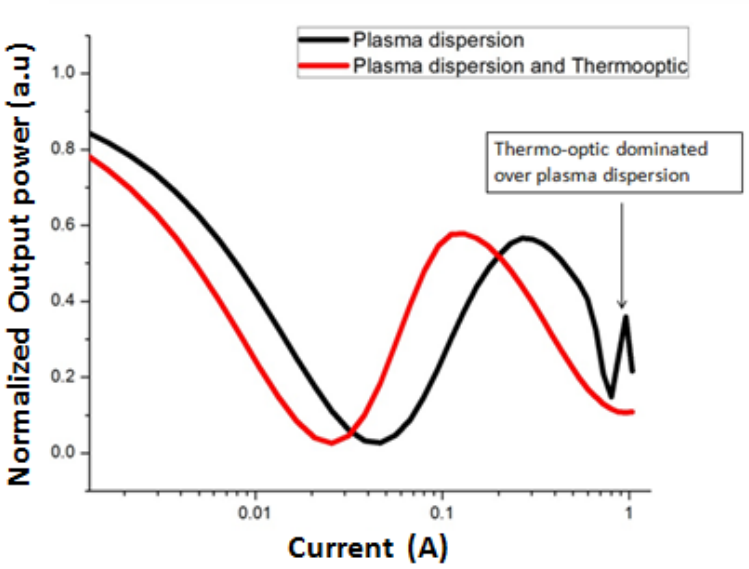

Figure 3.24: Power characteristics of Mach-Zehnder modulator. Thermo-optic effect due to self heating and plasma dispersion in a single package of simulations.

This technique have some advantages like low loss, thermo-optic effect is relatively faster and localized heating is possible instead of spreading the energy.

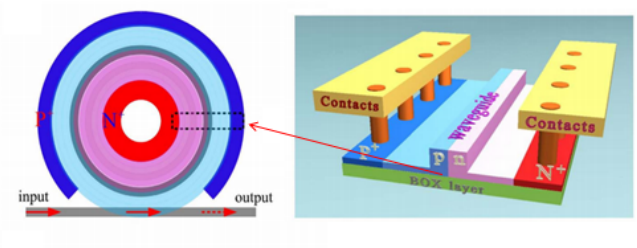

Figure 3.25: Plasma dispersion and thermo-optic effect by exploiting the carrier depletion [23].

3.3 Photonic wire rib waveguide

Now the computation is extended to photonic wire rib waveguide. The miniaturization enhances the speed of operation. Moreover the bending loss is minimum for this

structure. At the same time the photonic wire(sub micron) dimensions are highly polarization dependent. Consider the following structure for photonic wire rib waveguide

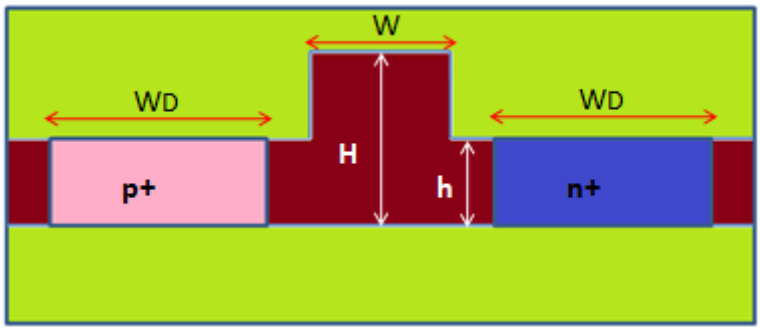

Figure 3.26: Parameters for photonic wire rib waveguide dimension

This particular structure is designed for single-mode operation at one particular polarization. Here the parameters $H = 250nm, h = 125nm, W = 500nm$ are chosen in such a way that this will be single mode for TE polarization . The doping parameters are arbitrarily chosen as both doping concentrations $p = n = 5 \times 10^{19} cm^{-3}$ and $WD = 1\mu m$.The doping profile is diffusion and the discretization (mesh size) used for computation is 5nm.

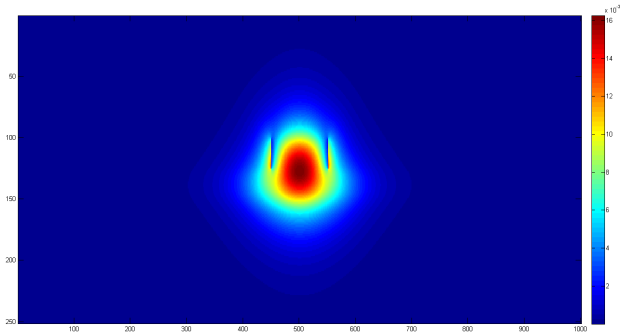

Figure 3.27: Mode profile for TE polarization,with $H = 250nm, h = 125nm, W = 500nm$,$WD = 1\mu m$.

The effective refractive index for TE mode is calculated using semi vectorial mode solver and the same compared using lumerical mode solver by importing the computed refractive index profile.

The effective refractive index parameters

At Zero applied bias:

Using Semi-vectorial mode solver - 2.7358

Using Lumerical mode solver -2.7293

At 1 volt applied bias:

Using Semi-vectorial mode solver - 2.7317

Using Lumerical mode solver -2.7267

From the above observations it is clear that there are significant variations in the values of effective indices. The solution for this is to incorporate full vectorial mode solutions along with poisson's solver. The reason for going in to full vectorial mode solver is, at photonic wire dimension the modes are highly coupled and it is very difficult to distinguish TE and TM modes seperately.

CHAPTER 4

Summary and Conclusions

Computation and analyses of p-i-n waveguide phase shifters on various cross-sections (large cross-section rib waveguide, reduced cross-section rib waveguide and photonic wire waveguide) were carried out. All the computation results are compared with commercial software (T-CAD Medici, Lumerical). Equilibrium, steady state and transient characteristics are explained based on the small signal model of diode. Steady state thermo-optic characteristics of large cross-section rib waveguide p-i-n phase shifter analyzed and compared to the experimental results. Modal characteristics of photonic wire rib waveguide is found slightly different from the result obtained by commercial simulation tool. We assume, this could be due to the semi-vectorial mode solver which we used to solve the optical characteristics of the waveguide. This can be improved by incorporating the Full-Vectorial mode solver.

4.1 Outlook

Detailed study of photonic wire rib waveguide can be carried out by combining full vectorial mode solver. This thesis work can be used for studying the depletion mode p-n phase shifter (based on traveling wave electrode) by extending it to 3D. Steady state thermo-optic effect of the device can be studied completely by incorporating the effects of contact resistance to the package. Transient thermo-optic effect also has to be investigated thoroughly for high speed device applications. Incorporation of Newton's computation method in this package will make the convergence more faster at higher injection case.

REFERENCES

[1] http://www.chipdesignmag.com/bursky/?p=95

[2] M. T. Bohr,"Interconnect scaling-the real limiter to high performance ulsi",in Electron Devices Meeting, 1995, International IEEE, 1995, pp 241-244.

[3] http://osa opn.org/home/articles volume20/ issue6/features green silicon photonics

[4] R. Soref, "Applications of silicon-based optoelectronics", MRS Bull.,pp.20 -24, Apr. 1998.

[5] J.-P. Colinge, "Silicon-on-Insulator Technology Materials to VLSI". Boston, MA: Kluwer Academic, 1991.

[6] L. Peters, "SOI takes over where silicon leaves off", Semiconduct. Int.,vol. 16, pp. 48 51, 1993.

[7] B. Jalali, "Senior Member, IEEE, S. Yegnanarayanan, T. Yoon, T. Yoshimoto, I. Rendina, and F. Coppinger,Advances in Silicon-on-Insulator Optoelectronics',IEEE journal of selected topics in quantum electronics , vol. 4, NO. 6, November/December 1998.

[8] M. Takatsuji, "Quantum theory of the optical kerr effect", Physical Review, vol.155, no. 3, p. 980, 1967

[9] W. Franz,"Influence of an electric field on an optical absorption" edge, Z. Naturforsch,13a, vol. 484, 1958.

[10] G. Cocorullo, M. Iodice, and I. Rendina, "All silicon fabry perot modulator based on the thermo optic effect", Optics letters, vol. 19, no. 6, pp. 420 422, 1994.

[11] R. Soref and B. Bennett, "Electrooptical effects in silicon", Quantum Electronics,IEEE Journal of, vol. 23, no. 1, pp. 123 129, 1987.

[12] Laurent Vivien, Lorenzo pavesi "Hand book of silicon photonics chapter-9 optical modulation" pp-453,454

[13] D. J. Thomson, F. Y. Gardes, J.-M. Fedeli, S. Zlatanovic, Y. Hu, B. P. P. Kuo, E. Myslivets, N. Alic, S. Radic, G. Z. Mashanovich et al., "50 Gbps silicon opticalmodulator", Photonics Technology Letters, IEEE, vol. 24, no. 4, pp. 234 236,2012.

[14] C. Tang, G. Reed, A. Walton, and A. Rickman, "Low loss, single model optical, phase modulator in simox material", Lightwave Technology, Journal of, vol. 12, no. 8, pp. 1394 1400, 1994.

[15] Francesco G. Della Corte, Maurizio Esposito Montefusco,Luigi Moretti,Ivo Rendina, and Giuseppe Cocorullo "Temperature dependence analysis of the thermo optic effect in silicon by single and double oscillator models",Journal of Appl.phy,vol 88,dec 2000.

[16] Samarelli,Antonio 2011, Phd. thesis "Microring resonators in SOI", chapter4 , pp 81 82

[17] Allan D. Kraus Adrian Bejan. HEAT TRANSFER HANDBOOK. JOHN WILEY SONS, INC., 2003.

[18] Xi Xiao, Haihua Xu, Yingtao Hu, Zhiyong Li, Yuntao Li, Yude Yu and Jinzhong Yu.,"Toward high-speed, low-cost, on-chip silicon optical interconnects" 19 January 2011, SPIE Newsroom.

[19] Matthew. N. O. Sadiku,Elements of electromagnetics, Third edition,chapter 4 and 5,pages 103 ,182

[20] "Computational Electronics" by Dragica vasileska,chapter4,pp 161 162.

[21] Francesca Magno, Francesco Dell Olio and Vittorio M. N. Passaro,"Multiphysics Investigation of Thermo optic Effect in Silicon on Insulator Waveguide Arrays",Excerpt from the Proceedings of the COMSOL Users Conference 2006 Milano.

[22] http://nanohub.org/resources/4895/download/pn diode series resistance

[23] Xianyao Li, Hao Xu, Xi Xiao, Zhiyong Li, Yude Yu, and Jinzhong Yu, "Fast and efficient silicon thermo optic switching based on reverse breakdown of pn junction", February 15, 2014 ,Vol. 39, No. 4 , OPTICS LETTERS.

[24] P.Sakthivel, MS Thesis 2014,IIT Madras, "Simulation and Fabrication of Diffusion Doped PIN Structures for Application in Optical Interconnect Devices".

[25] M.Chaitanya Kumar, M.Tech thesis 2013,IIT Madras "Numerical Analysis of Integrated Optical PIN phase Modulator".